



Binary collisions of drying maltodextrin droplets and glass beads

N.M. Eijkelboom^a, V.J. Rang^a, S. Breevaart^b, R.M. Boom^a, P.F.C. Wilms^a, M.A.I. Schutyser^{a,*}

^a Laboratory of Food Process Engineering, Wageningen University and Research, P.O. Box 17, 6700, AA Wageningen, the Netherlands

^b Information Technology Group, Wageningen University and Research, P.O. Box 8031, 6700, EW Wageningen, the Netherlands

ARTICLE INFO

Keywords:

Single droplet drying
Sticking
Agglomeration
Locking point
Model

ABSTRACT

Spray drying is often used in combination with agglomeration to produce powders with good functional properties, yet the mechanistic understanding of this agglomeration is limited. This research is a fundamental study into the binary collision dynamics underlying agglomeration, identifying specific collision outcome regimes. A sessile single drying droplet was subjected to collisions with glass beads. For maltodextrins with a dextrose equivalent of 6, 21 and 38, collisions were performed at different time points in the drying process. A shift in the collision outcome was observed during drying. The transition from merging as sole collision outcome to a regime where also sticking and bouncing were observed was linked to the locking point of the drying droplet. The sticking regime was observed from 0.75 to 1.5 $t_{\text{collision}}/t_{\text{lock}}$. This indicates that precise timing of the collisions between drying droplets and dry fines is needed to optimize the agglomeration within a spray dryer.

1. Introduction

During spray drying a liquid feed is atomized into droplets which are then transformed into a dried and agglomerated powder. Spray dried powder particles can be characterized by their size and degree of agglomeration, which co-determines their techno-functional properties (Buchholz et al., 2022). Agglomeration can be enhanced after spray drying by using a spray fluidized bed. This process has already been extensively studied, and models have been developed to simulate the process (Du et al., 2022; Terrazas-Velarde Korina et al., 2011). However, agglomeration can also occur within a spray dryer. After atomization, droplets in a spray can collide. With an increasing frequency of droplet collisions the degree of agglomeration increases, thereby improving the rehydration properties of the final powder (van Boven et al., 2023). The presence of dried particles that have hardly agglomerated is less desired in spray dried powders, as these small particles negatively affect the flowability, dispersibility and handling properties (Fröhlich et al., 2021).

During spray drying, small particles, also called fines, are usually recovered during subsequent fluidized bed drying, and are recirculated into the spray dryer, where they can enhance the agglomeration by colliding with drying droplets (Williams et al., 2009). The collision between a fine particle and a drying droplet can lead to merging, sticking or bouncing off each other (van Boven et al., 2023). When the drying droplet is still very liquid, the fine particle will generally merge with the

droplet, leading to one single dried circular particle. At later stages in the drying process, the droplet is more rigid, and the fine particle may bounce off, which does not lead to any agglomeration. Successful collisions are those that result in an intermediate between merging and bouncing: the fine particle sticks onto the surface of a droplet but does not (fully) merge with it. Several of these sticking collisions lead to the formation of agglomerated powder particles which is therefore desired. During spray drying, recirculation of fines is done to enhance the formation of agglomerates during so-called nozzle zone agglomeration, but this is hitherto empirical and needs to be adjusted for every ingredient (Fröhlich et al., 2023; van Boven et al., 2023). Better mechanistic understanding of the collision process between particles and drying droplets is important for finding rational guidelines for nozzle zone agglomeration.

It is virtually impossible to obtain this mechanistic understanding on droplet-droplet and droplet-particle collisions within a spray dryer, as countless collisions occur simultaneously at different stages of the drying process. Earlier research focused primarily on binary collisions of wet droplets (Finotello et al., 2018a; García Llamas et al., 2024), however, for agglomeration especially collisions between drying droplets and fine particles are relevant. Fewer studies focused on droplet-particle collisions. For example, collisions were studied between water droplets and glass beads (Pawar et al., 2016). Unfortunately this does not allow the evaluation of the drying stage on the outcome of the collisions, as sticking and bouncing is not observed with water droplets. The

* Corresponding author.

E-mail address: maarten.schutyser@wur.nl (M.A.I. Schutyser).

<https://doi.org/10.1016/j.jfoodeng.2024.112110>

Received 27 February 2024; Received in revised form 5 April 2024; Accepted 26 April 2024

Available online 2 May 2024

0260-8774/© 2024 The Author(s). Published by Elsevier Ltd. This is an open access article under the CC BY license (<http://creativecommons.org/licenses/by/4.0/>).

observation of different collision regimes, i.e. merging, sticking and bouncing, requires collisions between drying solute-containing droplets and solid particles, which has not been studied yet. Therefore, in this study, we examine binary collisions between drying sessile droplets of maltodextrin solutions and small glass beads, representing the fines that are conveyed in a hot air stream in a spray drying process.

We use a modified single droplet drying (SDD) setup to study these binary collisions. Single droplet drying (SDD) studies are common to investigate the impact of the drying conditions on heat sensitive components or particle morphology development, and thereby improve our understanding of the spray drying process (Eijkelboom et al., 2023a). Previous SDD research has shown that the choice of the solute and the drying conditions both influence skin formation and the subsequent development of the morphology of the drying droplets (Eijkelboom et al., 2023b; Siemons et al., 2020). For example, maltodextrins with a high dextrose equivalent (DE) show later locking points and give different droplet morphology than maltodextrins with a low DE. In addition, the skin of dried droplets made with high DE maltodextrin was predominantly viscous, while those with low DE maltodextrins formed an elastic skin (Siemons et al., 2020). These differences in locking point and rheological properties of the skin are expected to also influence the sticking behavior after a collision between a drying droplet and a particle.

The objective of this study is to identify the regimes for merging, sticking and bouncing with colliding drying droplets and particles. For this we characterize the drying droplet-particle collision behavior for maltodextrins of varying dextrose equivalent, i.e. DE6, 21 and 38, and glass beads. To create the unique possibility to investigate collision between a drying droplet and a dry particle, a single droplet drying system is adapted, by adding a dispensing system for glass beads, upstream in the air flow. The collisions are observed using high-speed imaging, and the collision outcomes are coupled to the collision parameters, drying conditions and evolving viscoelastic properties of the drying droplets. To relate the collision outcomes to the transient viscoelastic properties of the surface of the drying droplets, we employ a previously developed model for single droplet drying (Eijkelboom et al., 2024). This drying model builds on work earlier developed by (Siemons et al., 2022) and predicts the transient rheological properties of maltodextrin solutions during drying as function of the drying time and location inside the droplet.

2. Materials and methods

2.1. Sample preparation

Maltodextrin with a DE of 6, 21 or 38 (MD6, MD21 and MD38, respectively) (Roquette Frères, France) was added to demi-water and stirred for 30 min to obtain transparent 20% (w/w) solutions. The molecular weight distribution of the maltodextrins can be found in Appendix A (Figure A.1).

2.2. Single droplet drying with collisions

The single droplet drying platform used in this study is an extended version of the platform used in previous work (Eijkelboom et al., 2024) and is schematically illustrated in Fig. 1 (Technical Development Studio, Wageningen, the Netherlands). Before a droplet was dispensed, the drying tunnel was preheated for 30 s using air of 80 °C with a flow rate of 10 L/min (0.4 m/s) with the camera backlight (PFBR 150SW MN (CCS Inc., Japan) with ½" x 12", flexible fiber optic light guide (Edmund Optics, United States) and 28 mm fiber-lite focusing assembly for hybrid/semi-rigid (Edmund Optics, United States)) turned off. Next, the air flow was stopped to allow the drying table (i in Fig. 1) to cool to 50 °C. When the drying table was at 50 °C, the camera backlight was turned on. To prevent extensive heating of the drying tunnel by the light source, the glass in between the light source and the drying tunnel was

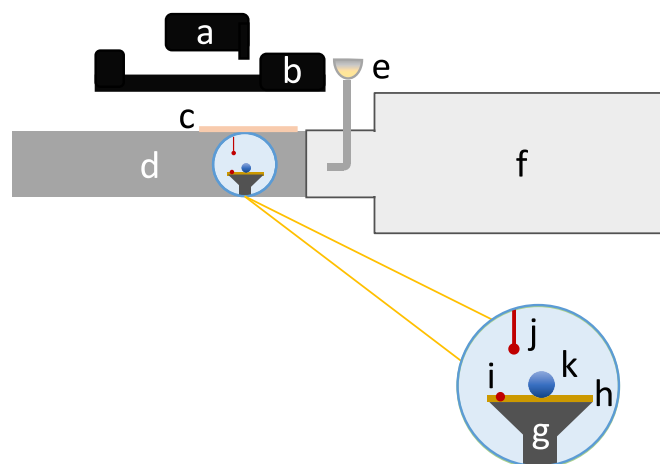


Fig. 1. Schematic overview of the sessile single droplet drying platform with dispenser (a), stroboscope (b), automated shutter (c), drying tunnel (d), powder reservoir (e), electric heating block (f), drying table (g), hydrophobic tape (h), thermocouple to measure contact surface temperature (i), thermocouple to measure air temperature near the droplet (j) and droplet (k).

covered with a heat repellent foil that blocks infrared radiation but allows most of the visible light to pass through (GSW® Ice Cool super plus 78 Extern, Raamfoliewebshop, the Netherlands).

A single droplet (initial radius of $200 \pm 15 \mu\text{m}$) was dispensed using a PipeJet® NanoDispenser (BioFluidix, Germany) equipped with 500-S, coated PipeJet® Pipes (BioFluidix, Germany). A stroboscope (BioFluidix, Germany) connected to BioFluidix Controle Software V2.9 (BioFluidix, Germany) was used to control the droplet volume. The droplet was dispensed onto a piece of PTFE coated glass fabric (PTFE glass fabric 0.18 AD, self-adhesive, High-tech-flon, Germany) to attain an almost spherical droplet. Once the droplet was dispensed, an automated shutter covered the small opening at the top of the drying tunnel, preventing the loss of hot air during drying. To dry the droplet, dry air (absolute moisture content of 3.5 g/kg) with a temperature of 80 °C and a flow rate of 10 L/min (0.4 m/s) was supplied to the droplet for 30 s. These conditions represent the outlet air of a spray dryer, and result in a drying rate allowing the accurate investigation of different collision regimes. The temperatures of the drying table and of the air in the drying tunnel (6 mm above the drying table) during these 30 s are indicated in Fig. 2.

To introduce fine particles in the airstream and induce collisions, a funnel was employed to dose the particles close to the outlet of the heating blocks. For every experiment, around 25 mg of glass beads (70–110 μm , density of 3.22 kg/m³, EPCCE Bouwstoffen B.V., the Netherlands, see Appendix B Figure B.1 for the exact size distribution) were added into the funnel. The particles were released using an automated control system. At a pre-selected time (1–10 s, with 1 s intervals), the beads flowed down the funnel and entered the heated air stream. The

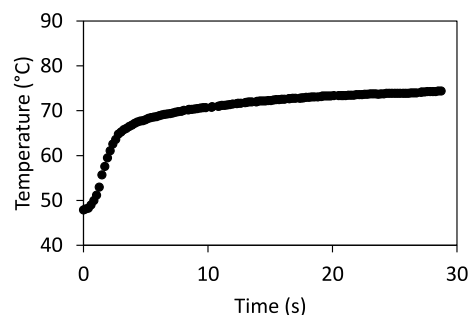


Fig. 2. Temperature of the drying air near the droplet (j in Fig. 1) as applied during the drying experiments in this research.

beads were entrained by the air stream and travelled towards the drying droplet. A few of these collided by chance with the drying droplet. The total number of collisions observed for droplets with MD6 was 106, for droplets with MD21, 226, and for droplets with MD38, 99.

The drying process and collisions were recorded with a high-speed camera (C-VIT, AOS Technologies AG, Switzerland) with a VZMTM 1000 Zoom Imaging Lens (Edmund Optics, Japan). Recording occurred in three blocks with different frame rates: before the collisions, during the collisions, and after the collisions. Before and after the collisions the camera operates at a frame rate of 100 fps, while a frame rate of 10,000 fps is used during the collisions. The movies are used to visually observe the locking point, i.e. the first point at which shape deviation from a sphere is visually observed (Siemons et al., 2020). A MATLAB (MATLAB R2018b, MathWorks, United States) image analysis script was used to determine the droplet size until the locking point. The collision outcomes (merging, sticking or bouncing) were observed with the high-speed clips. The clips were analyzed with a MATLAB (MATLAB R2018b, MathWorks, United States) image analysis script to determine the collision speed, the collision angle and the impact parameter. The collision angle was determined relative to the surface contact line of the sessile droplet (Fig. 3A). The measurement was performed with the camera footage and was determined based on the exact droplet shape at the time of collision. Only collisions with a collision angle between 0° and 90° were taken into account. To calculate the impact parameter (B), a slightly adapted version of the definition as generally used for the impact parameter between two free-flying droplets is used (Finotello et al., 2018a). Assuming that the path of the glass beads is parallel to the drying table, the impact parameter (B) was defined as the distance between the center of the droplet and the bead (b), normalized by the height of the drying droplet (h_d) and the diameter of the bead (d_b):

$$B = \frac{2b}{h_d + d_b} \quad (1)$$

As a result, the impact parameter can have values between -1 and 1 (Fig. 3B); a value of zero implies a collision where the centers of both particles are on the trajectory of the particle, a value of 1 indicates a collision at the top of the droplet, and a value of -1 indicates a collision at the bottom of the droplet.

2.3. Single droplet drying model

To predict the drying behavior and rheological properties of the drying droplet, we used a model that was developed earlier by (Siemons et al., 2022), and that was adapted as described in earlier work (Eijkelboom et al., 2024; Eijkelboom et al., 2023b). The model is a one-dimensional (1D) effective diffusion drying model, considering the droplet to be a spherical cap. This cap is divided into numerical shells of the same volume, and evaporation and heat flux is calculated per shell. For a full description of the model and equations we refer to our earlier work (Eijkelboom et al., 2024; Eijkelboom et al., 2023b; Siemons et al., 2022). The external mass transfer coefficient of the model was calibrated using the data of a water droplet without solute (no internal diffusion limitation) drying under the exact same conditions as all other experiments performed in this research. This indicated that the external mass transfer coefficient had to be adapted to $\beta_{ext, sessile} = 0.15 \beta_{ext, sphere}$ (Appendix C Figure C.1).

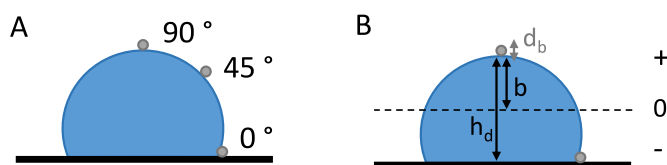


Fig. 3. Schematic representation of the determination of the collision angle (A), and the impact parameter (B).

2.4. Data analysis for the collision outcomes

For the collision outcomes, data analysis was performed using Python (Python Software Foundation, United States) (van Rossum and Drake, 1995) using external libraries for data handling (McKinney, 2010; McKinney, 2010), statistical analysis (Seabold and Perktold, 2010; Virtanen et al., 2020) and data visualization (Hunter, 2007). Reproducible computational workflows were established using Jupyter Notebooks (Project Jupyter, United States) (Kluyver et al., 2016), which can be made available upon request.

Kernel density estimation is used to generate probability plots. To compare the average collision speed, the collision angle and the impact parameter between the droplets with different maltodextrins and between the different collision outcomes, a two-way ANOVA followed by a Tukey HSD post-hoc test was performed. Assumptions of ANOVA were validated through Shapiro-Wilk Test for normality, visual inspection of Q-Q plots and Levene's test for homogeneity of variances.

3. Results and discussion

3.1. Skin formation of the drying maltodextrin droplets

The visually observed locking point is often linked to the skin formation point, the point in time when a solute-rich skin has formed at the outside of the droplet. As the formation of such a skin is expected to influence the collision outcomes, the locking point is expected to be an important parameter to characterize collisions. For the specific settings applied in this research, the locking points of drying droplets containing MD6, MD21 and MD38 were observed at 3.1 (± 0.3), 4.8 (± 0.6) and 6.6 (± 0.3) s, respectively. Previous research into the drying behavior of maltodextrins already revealed an earlier locking point for droplets containing a maltodextrin with lower DE values. A lower DE value also results in a higher moisture content at the locking point and a slower temperature increase after the locking point. There are also differences in skin development and morphology: a solute with a low DE value develops a skin that quickly acquires elasticity, resulting in smooth, hollow particles. A solute with high DE values results in the formation of a more flexible and more viscous skin which generally leads to denser and more wrinkled particles (Eijkelboom et al., 2023b; Siemons et al., 2020).

3.2. Collisions between sessile drying droplets and glass beads

When a glass bead collides with a sessile drying droplet, three different types of results can be observed. The first possibility is that the droplet and the particle merge, when the glass bead collides with the droplet and sinks into it (Fig. 4, Appendix D Video 1). The second possibility is sticking. In this case, the glass bead collides with the droplet and remains located at the surface of the droplet (Fig. 4, Appendix D Video 1). The third possible result is bouncing: the glass bead collides with the droplet, but is taken up by the airflow again (Fig. 4, Appendix D Video 1). Supplementary video related to this article can be found at <https://doi.org/10.1016/j.jfoodeng.2024.112110>

Differences in rheological properties of maltodextrins with different DE values are expected to influence the collision outcomes for a drying droplet and a dry particle. To investigate this, the collision outcomes are studied for three different drying maltodextrins (Fig. 5A) as a function of collision time. We observed that the start of the sticking regime was delayed when using a maltodextrin with a high DE value. As a high DE value results in a later locking point, it takes longer until the droplet is dry enough that not all collisions will result in merging. Also, the onset of the bouncing regime is later, as the skin is more viscous compared to the more elastic skins formed for low DE maltodextrins. Due to the slower changes in the rheological properties, the merging and sticking regimes are also spread over a longer time.

As the formation of a skin will influence collision outcomes, the

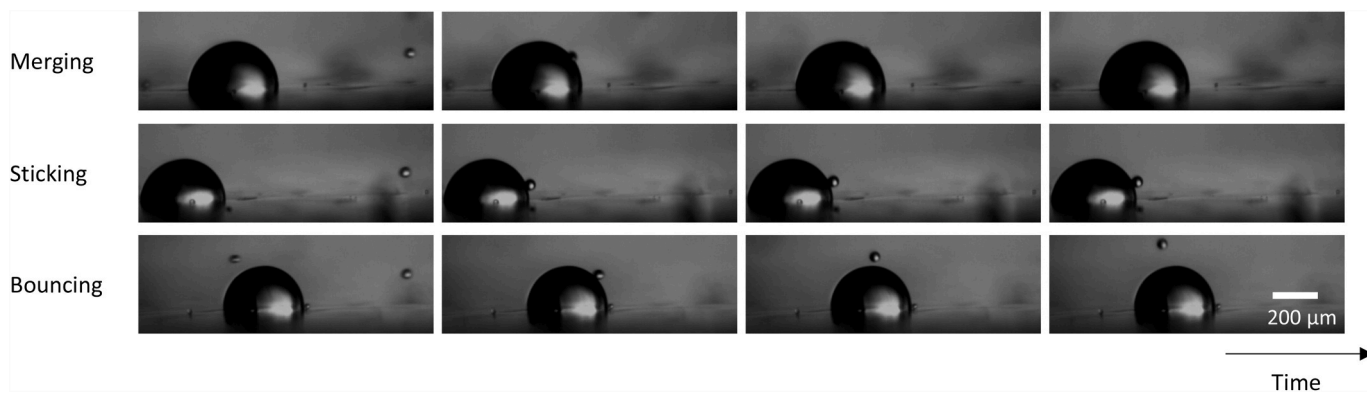


Fig. 4. Different possible collision outcomes when a glass bead hits a sessile drying droplet.

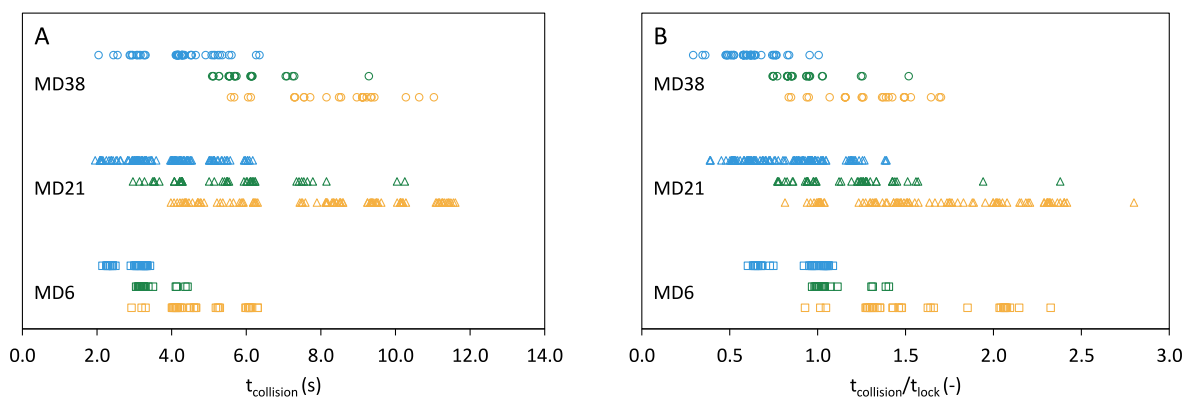


Fig. 5. Collision outcomes over time (A) and over normalized time (B) for maltodextrin DE6 (squares), DE21 (triangles) and DE38 (circles), with merging indicated in blue, sticking in green, and bouncing in yellow.

collision time was normalized with respect to the average locking point time (Fig. 5B). After normalization, the distribution of collision outcomes for different maltodextrins shows more similarity, indicating the relevance of the locking point in the collision process. Merging is already observed from the start of the drying process but continues until after the locking point. For all three DE values, the first observation of sticking is at $t_{collision} \approx 0.75 t_{lock}$, with this onset point of the sticking regime being somewhat earlier if the DE value is higher. Based on the experiments, the endpoint of the sticking regime is at $t_{collision} \approx 1.5 t_{lock}$ for all DE values, except for a few outliers. By the time that sticking is observed, some collisions also result in bouncing. Bouncing then continues to be observed from the locking point onwards and becomes the only type of collision outcome after the sticking regime has ended.

There are several factors influencing the collision outcome, and since

not all of those can be controlled in our experiments, the collision outcomes are partially stochastic. Local differences in skin properties due to inhomogeneous drying of the droplet, small variations in locking points, as well as differences in droplet and glass bead size will add a level of randomness to the outcomes. Probability plots can be generated based on kernel density estimation to visualize the chance of observing a specific collision outcome (Fig. 6). The probability plots indicate that the maximum probability of observing sticking differs per maltodextrin type, with the highest probability observed for MD38. These differences might be caused by the rheological properties of the skin that is formed. The viscous skin that is formed for maltodextrins with a high DE value promote sticking more than the elastic skins for maltodextrins with a low DE value (Siemons et al., 2020). Note that, because of the relatively limited sample size for each point in time, the kernel density algorithm

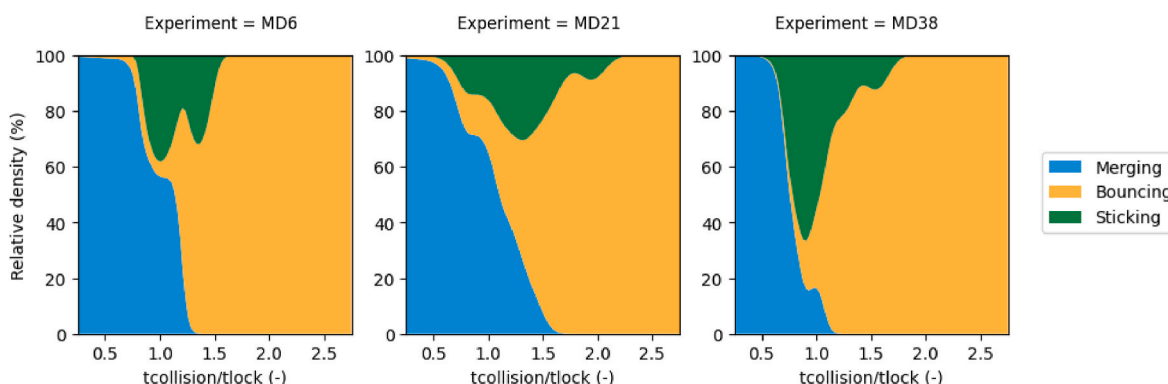


Fig. 6. Stacked area charts for different maltodextrins based on kernel density estimation values relative for each collision outcome across $t_{collision}/t_{lock} (-)$.

also estimates the (small) chance of observing a specific collision outcome at a point in time when it was not observed experimentally. The probability plots for example show a slight probability of observing bouncing already before a probable collision outcome of sticking is observed.

3.3. Influence of the collision speed on collision outcomes

At the times when a collision could result in several outcomes, it is expected that other factors than drying time might determine the collision outcome. For colliding liquid droplets, it is known that the Weber number, the ratio of the inertial forces to the cohesion forces such as surface tension, co-determines the collision outcome. Since the collision velocity is a factor in the inertial forces, it impacts the Weber number and hence the collision outcome of wet collisions (Finotello et al., 2018b; Li et al., 2016; Qian and Law, 1997). It is expected that collision velocity will also influence the outcome of a collision between a drying droplet and dry particle.

Although the speed of the air entraining the colliding particles was kept constant at 0.4 m/s, differences in collision speed were observed. The observed speeds ranged from 0.3 to 3.0 m/s, which is similar to the relative collision speeds observed within a spray dryer, i.e. 0.5–3.5 m/s, as mentioned in other research (Hussain et al., 2022; Li et al., 2016). However, within the range of collision speeds that we observed, the speed had no clear impact on the collision outcome. This is also evidenced by the distributions of the frequency of the types of outcomes as function of the collision speed, for all different collision outcomes and maltodextrin types (Fig. 7). Only between MD6 and MD21 a significant difference in speed for bouncing outcomes was observed (mean difference 0.25 m/s, $p = 0.036$).

Pawar et al. (2016) did observe an influence of the Weber number on collision outcome for collisions between solute-free water droplets (initial diameter of $2939 \pm 125 \mu\text{m}$) and glass beads (diameter of 2500 or 4000 μm). The relative velocity in their experiments ranged from 0.065 to 1.15 m/s, partially overlapping with our collision speeds. Within the work of (Pawar et al., 2016), it was observed that the collision outcomes changed from resulting in agglomeration to showing stretching separation upon increasing the Weber number. The difference in the (relative) sizes of the droplet and particle compared to our experiments could have contributed to the different observations of the impact of the Weber number. The smaller droplets (initial diameter of 400 μm) and glass beads (diameter of 30–110 μm) in our experiments result in a lower Weber number, possibly being below the limit to observe an influence on collision outcome. For these smaller particles, the relative velocity differences may therefore not be important. In spray dryers, a similar size difference between drying primary particles and colliding fines is expected, but it remains to be verified if one can extend these observations.

3.4. Influence of the collision angle on collision outcomes

Previous research on binary collisions focused on free flowing, non-drying droplets, being uniform in shape and composition. The presence of a hot surface on which the sessile droplet is deposited, hinders the droplet from drying completely uniform. Therefore, the location of the collision, which can be indicated by the collision angle (Fig. 3A), could potentially influence the collision outcome in this situation. For MD21 a significant difference in collision angle distribution between bouncing and merging (mean difference of 8.9° , $p = 0.041$), and between bouncing and sticking (mean difference of 14.4° , $p = 0.012$) was observed, showing that a small collision angle more often resulted in bouncing. This could be when the lower part of the droplet, closer to the contact surface area, dries faster, leading to an earlier change from sticking to bouncing. Although no significant difference was observed for MD6, the trend of more frequent bouncing at a lower collision angle seems to be present (Fig. 8), but might be non-significant due to the lower sample size. The trend was not observed for MD38 (Fig. 8). The differences between the different maltodextrins could be a result of their different rheological properties. An elastic skin that quickly becomes glassy as for MD6 and MD21 will result in more bouncing, while the more viscous skin of MD38 still shows more sticking.

3.5. Influence of the impact parameter on collision outcomes

The impact parameter, as calculated from Eq. (1), was expected to influence the collision outcome. The impact parameter is related to the collision angle (Fig. 3), because they both take the position of the collision into account. Next to this, the impact parameter is based on the size of the droplet and bead, which in principle is kept constant in our experiments, but does show some natural variation.

Previous work on droplet-droplet interactions revealed that a change in impact parameter did influence the collision outcome, with a general trend of collision outcomes changing from reflexive separation, to coalescence, to stretching separation, to bouncing upon an increasing impact parameter (Finotello et al., 2018b; Qian and Law, 1997). The impact parameter was also found to impact the outcome of collisions between water droplets (initial diameter of $2939 \pm 125 \mu\text{m}$) and glass beads (diameter of 2500 or 4000 μm), with an increase in impact parameter resulting in the collision outcome changing from agglomeration to stretching separation (Pawar et al., 2016).

For the experiments performed in this study, there was, however, no influence of the impact parameter on the collision outcome (Fig. 9). For all different maltodextrins and outcomes, no significant differences in impact parameter distribution were observed. An important difference between the previous research and our current work is that previous research made use of two moving objects, while we use a stationary droplet. In previous research, the distance between the droplet centers

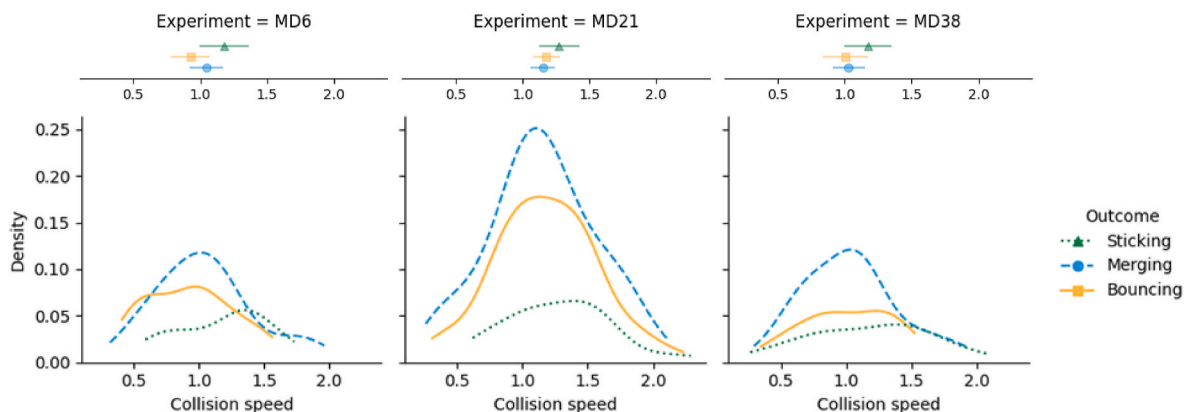


Fig. 7. Confidence interval and density plots for collision speed, comparing outcomes and experiments.

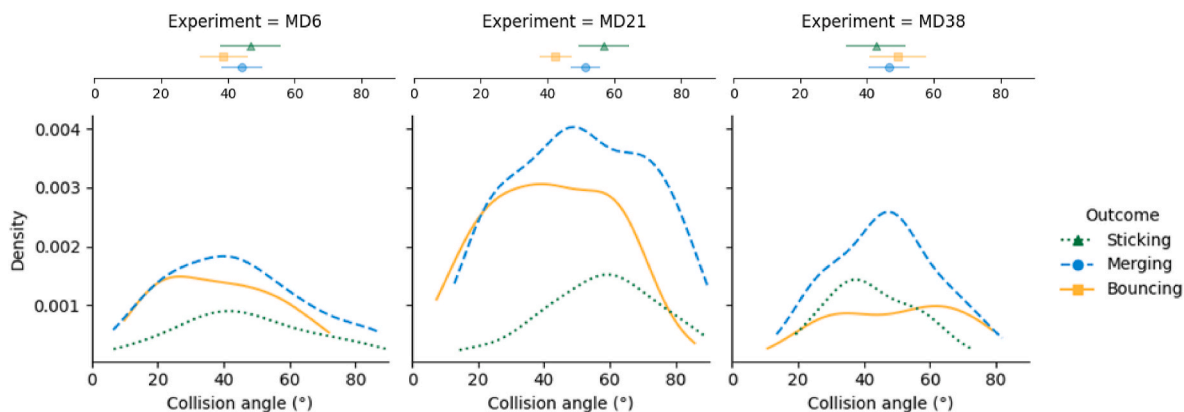


Fig. 8. Confidence interval and density plots for collision angle, comparing outcomes and experiments.

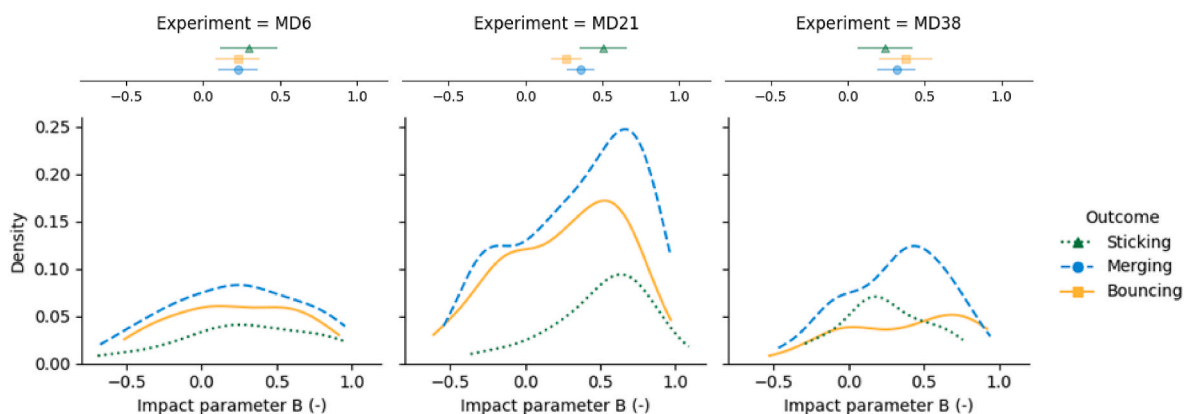


Fig. 9. Confidence interval and density plots for impact parameter, comparing outcomes and experiments.

was determined in the plane perpendicular to the relative velocity vector. Because of the stationary droplet in our work, and the assumption of the glass bead flying parallel to the surface that the droplet is sitting on, the relative velocity vector is constant in our case. The differences in experimental procedure and in the approach of obtaining the impact parameter might contribute to the difference in observed influence. In addition, the two-dimensional, instead of three-dimensional, observation of the collision outcome could result in small mismatches between the real and observed impact parameter, if the glass bead does not move in the center plane. As the collision angle and impact factor are highly correlated factors, the difference in the correlations found with collision outcomes is surprising. This most likely has to do with the mathematical concept behind the kernel density estimation. The estimation values are relative to the total area under the density curve, and differs between the contact angle and impact parameter due to different scales on the x-axis.

3.6. Modelling

Based on the experimental results, the time of collision with respect to the locking point of the drying droplet is the main parameter to indicate the collision outcome. Experimental data showed that sticking generally occurs when $t_{\text{collision}}/t_{\text{lock}}$ is between 0.75 and 1.5, and the kernel density algorithm estimates this timeframe to be even a bit wider. To get a rough estimation if sticking can occur at a specified time, it would therefore be desired to predict the locking point of the drying droplet with a model. Previous work has already focused on the development of a sessile single droplet drying model to predict the change in droplet volume, (uniform) droplet temperature and rheological properties (Eijkelboom et al., 2023b; Siemons et al., 2022). This showed that,

for maltodextrins with different DE values, at the skin formation point the change in concentration of maltodextrin in the outer shell can be linked to specific rheological properties. The skin formation point was indicated by the steepest increase in the logarithmic value of the storage modulus ($\log G'$) in combination with a characteristic change in the loss factor ($\tan \delta$) (Siemons et al., 2022). Also the onset of the increase in droplet temperature has been linked to the locking point (Eijkelboom et al., 2023b). Therefore, having a single droplet drying model that properly predicts the drying behavior and change in rheological properties of the droplet as examined in our experiments, will help to make predictions on locking point and collision outcomes.

Calibration of the existing single droplet drying model with a pure water droplet showed us that the external mass transfer coefficient had to be adapted to $\beta_{\text{ext, sessile}} = 0.15 \beta_{\text{ext, sphere}}$ (Appendix C, Figure C.1.). This adapted model was applied for the different drying maltodextrin systems used in this research (Fig. 10).

The rapid temperature increase, steepest increase in $\log(G')$ and characteristic change in $\tan \delta$ happen, respectively, at 8.7, 8.8 and 9.0 s for MD6, MD21 and MD38. The trend of having a later locking point for higher DE values does align with the experimental results. Nonetheless, the predictions deviate quite substantially from the experimentally observed locking points (respectively 3.1 (± 0.3), 4.8 (± 0.6) and 6.6 (± 0.3) s). To find the cause of this deviation, sensitivity analyses were carried out for the external mass transfer coefficient and number of volumetric shells (results not shown). In case of the mass transfer coefficient, a larger mass transfer coefficient results in an earlier locking point, but it also results in a faster decrease in droplet volume, which no longer matches the experimental observations. Considering the good match between predicted droplet volume decrease and experimental results (Fig. 10), the external mass transfer coefficient was therefore

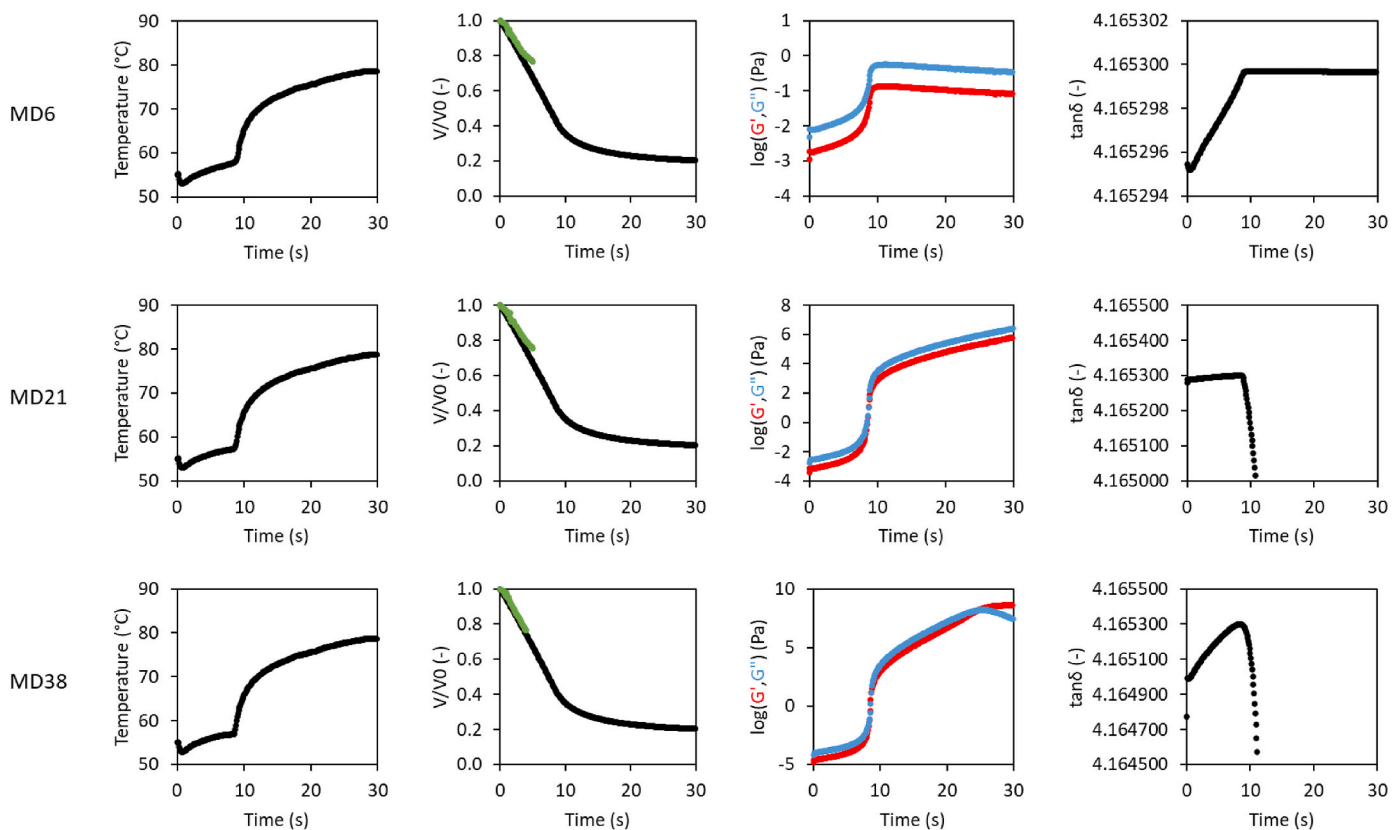


Fig. 10. Model predictions related to droplet temperature and volume development (including experimental data in green), and rheological development the outer volumetric shell of drying particles of 20% maltodextrin DE 6, 21 and 38 solutions, with the mutual solute-water diffusion coefficient based on the Darken relation.

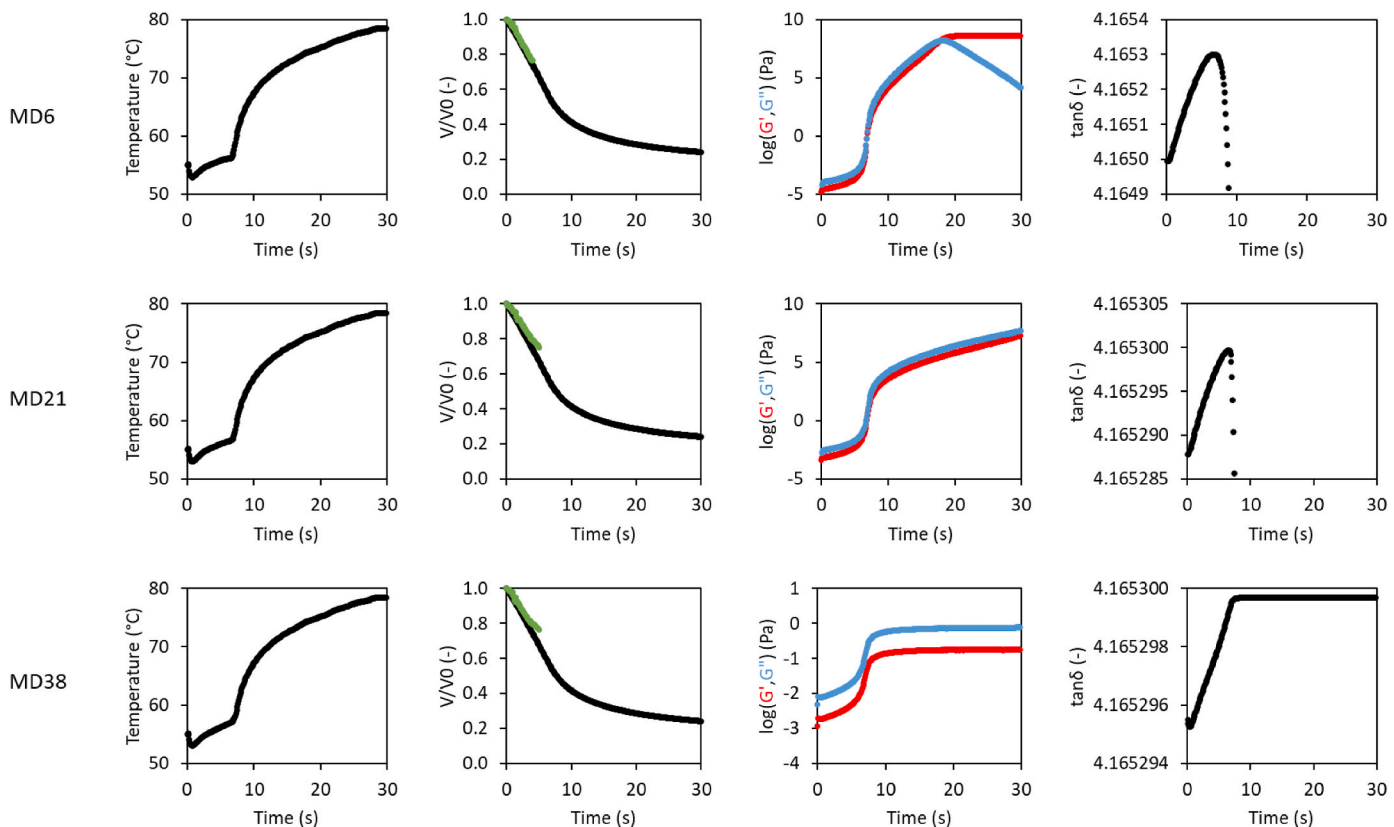


Fig. 11. Model predictions related to temperature, volume (including experimental data in green), and rheological development of drying particles of 20% maltodextrin DE 6, 21 and 38 solutions, with the mutual solute-water diffusion coefficient based on Räderer et al. (2002).

assumed to be correct. In the case of the number of volumetric shells, an increase in number of shells would make the simulation of a thin skin layer more accurate, and could thereby result in a different timing of characteristic changes in rheological properties. However, no such effect was observed. By using 40 volumetric shells, for MD6 the outer shell has a thickness of 0.80 μm and a moisture content of 0.54 g/g at the locking point. After increasing the number of volumetric shells to 400, the outer shell still had a moisture content of 0.52 g/g at the locking point, which is not a sufficient reduction to make a substantial difference. Another possible explanation for the differences between experiment and model could be a discrepancy between the calculated and actual mutual solute-water diffusivity. A difference in the mutual solute-water diffusivity in the droplet would result in the same, correct, predictions for the total volume decrease, but would influence the timing of the changes of the properties of the outer shell of the droplet. The current model uses the mutual diffusion coefficient that is based on the Darken relation to calculate the internal water diffusion. Alternatively, one can use the formula obtained by (Räderer et al., 2002) which is based on experiments with maltodextrin DE33 (Fig. 11). This formula has also been applied in a previous single droplet drying model by (Perdana et al., 2013). The diffusion coefficients as a function of the water content based on the Darken relation for MD21 and based on the relation suggested by (Räderer et al., 2002) can be found in Appendix E, Figure E.1.

With this adapted version of the model, the predicted rapid temperature increase, steepest increase in $\log(G')$ and characteristic change in $\tan \delta$ all happen at 6.8 s, independent of the DE value of the maltodextrin. For MD38, this aligns well with the experimentally observed locking point. For MD6 and MD21, the predicted locking points are closer to the experimental locking point than for the model with the mutual solute-water diffusion coefficient based on the Darken relation, but do still deviate. It is known that the diffusion is dependent on the type of solute present, with a general decrease of the diffusivity of water as the molecular weight of the solute increases (Adhikari et al., 2002). However, maltodextrins consist of a mixture of molecules with different molecular weights and the specified DE value thus represents an average. Unfortunately no information is presented regarding the true molecular weight distribution of the MD used by (Räderer et al., 2002). Nonetheless, it is expected that the molecular weight distribution of their maltodextrin DE33 is closest to our MD38. In the case of MD21 and MD6, the average molecular weight will be higher and will thus show a lower diffusivity than what is currently predicted. This will result in an earlier locking point, which is in line with the experimental observations. By using the diffusion equation as suggested by (Räderer et al., 2002), the drying model already gives a decent first indication of the locking point for maltodextrins with a high DE value. The model can already be used to get a first indication of the sticking regime that ranges from 0.75 to 1.5 $t_{\text{collision}}/t_{\text{lock}}$. In the future, more accurate determination of the mutual solute-water diffusivity in different solute systems could help optimize locking point predictions.

4. Conclusion

To obtain better insight in the collision behavior between drying droplets and fine particles during spray drying, a sessile single droplet drying platform was extended to assess binary collision outcomes between a drying droplet and glass beads. We used drying droplets containing different maltodextrins (DE 6, 21 and 38) and performed collisions at several timepoints throughout the drying process.

Outcomes of the binary collisions depended on the timing of the collision. Collisions at the start of the drying process only resulted in merging, while later in time also bouncing and sticking were observed. The transition from merging to other collision outcomes occurred at different absolute times, depending on the dextrose equivalent of the maltodextrin. For maltodextrins with increasing DE value, the transition to sticking and bouncing occurs later, because of the later locking points of these droplets. If the collision time was corrected for the locking

point, the different maltodextrins showed a similar sticking regime, ranging from 0.75 to 1.5 $t_{\text{collision}}/t_{\text{lock}}$. Due to the formation of a viscous, rather than an elastic, skin, the maximum probability to obtain sticking was higher for MD38 than for the lower DE maltodextrins.

For all investigated systems, the observed collision outcome over time is stochastic. For the viscous skin forming MD38 no significant impact of collision speed, collision angle or impact parameter on the collision outcome was observed. For low-DE maltodextrins that form an elastic, glassy skin, the collision angle had a minor impact on the collision outcome. Bouncing was more likely to result at low collision angles, i.e. where the droplet is in contact with the support surface and dries faster.

The impact of particle properties, like density, is still to be examined. For now, it is expected that the lower density of the fines in industrial spray dryers compared to the glass beads used in this work will result in more sticking. Work of (Hussain et al., 2022) indicated that in order to obtain sticking, the collision velocity needs to be below a specific critical velocity. A decrease in particle density results in an increase in this critical velocity, probably resulting in a larger range where sticking can be observed.

The collision time relative to the locking point is the key parameter to determine the collision outcome. It would therefore be of interest to predict the locking point time, and thereby have a prediction for the collision outcome, with a drying model. A numerical model that combines the drying of a single droplet with the rheological properties of the matrix was used to predict the locking point. The results were in reasonable agreement with the experimentally determined locking points. Especially the mutual solute-water diffusivity is found to play a major role, and accurate determination of the diffusion coefficient could further improve the locking point estimation.

The extended sessile single droplet drying platform allowed us to identify the different collision outcomes for drying droplets and particles. The found consistency of the sticking regime relative to the locking point provides a new step towards better control of agglomeration processes.

CRediT authorship contribution statement

N.M. Eijkelboom: Writing – review & editing, Writing – original draft, Visualization, Validation, Methodology, Investigation, Formal analysis, Conceptualization. **V.J. Rang:** Methodology, Investigation. **S. Breevaart:** Writing – review & editing, Visualization, Methodology, Formal analysis. **R.M. Boom:** Writing – review & editing, Supervision, Conceptualization. **P.F.C. Wilms:** Writing – review & editing, Supervision, Conceptualization. **M.A.I. Schutyser:** Writing – review & editing, Supervision, Funding acquisition, Conceptualization.

Declaration of competing interest

The authors declare that they have no known competing financial interests or personal relationships that could have appeared to influence the work reported in this paper.

Data availability

Data will be made available on request.

Acknowledgements

This work is an Institute for Sustainable Process Technology (ISPT) project, i.e. StAggloP (Project number: DR-50-15). Partners in this project are Corbion, Danone, dsm-firmenich, FrieslandCampina, University of Hohenheim, Wageningen University & Research and ISPT. This project is co-funded with subsidy from the Topsector Energy by the Dutch Ministry of Economic Affairs and Climate Policy. More information can be found at <https://ispt.eu/projects/stagglop/>. We would like

to thank the people from Technical Development Studio of Wageningen University & Research, especially Hans Meijer, Hans de Rooij and Jeroen de Pagter, for developing the single droplet dryer. We would also like to acknowledge Maurice Strubel for the HPLC measurements and Johannes Kingma for the preliminary work.

Appendix A. Supplementary data

Supplementary data to this article can be found online at <https://doi.org/10.1016/j.jfoodeng.2024.112110>.

References

- Adhikari, B., Howes, T., Bhandari, B.R., Yamamoto, S., Truong, V., 2002. Application of a simplified method based on regular regime approach to determine the effective moisture diffusivity of mixture of low molecular weight sugars and maltodextrin during desorption. *J. Food Eng.* 54, 157–165. [https://doi.org/10.1016/S0260-8774\(01\)00203-5](https://doi.org/10.1016/S0260-8774(01)00203-5).
- Buchholz, M., Haus, J., Pietsch-braune, S., Kleine, F., Heinrich, S., 2022. CFD-aided population balance modeling of a spray drying process. *Adv. Powder Technol.* 33 (7), 103636. <https://doi.org/10.1016/j.apt.2022.103636>.
- Du, J., Strenzke, G., Bück, A., Tsotsas, E., 2022. Monte Carlo modeling of spray agglomeration in a cylindrical fluidized bed: from batch-wise to continuous processes. *Powder Technol.* 396, 113–126. <https://doi.org/10.1016/j.powtec.2021.10.051>.
- Eijkelboom, N.M., Boven, A. P. Van, Siemons, I., Wilms, P.F.C., Boom, R.M., Kohlus, R., Schutyser, M.A.I., 2023a. Particle structure development during spray drying from a single droplet to pilot-scale perspective. *J. Food Eng.* 337. <https://doi.org/10.1016/j.jfoodeng.2022.111222>.
- Eijkelboom, N.M., Gawronska, K., Vollenbroek, J.M., Kraaijveld, G.J.C., Boom, R.M., Wilms, P.F.C., Schutyser, M.A.I., 2024. Single droplet drying with stepwise changing temperature-time trajectories: influence on heat sensitive constituents. *Food Res. Int.* 182. <https://doi.org/10.1016/j.foodres.2024.114194>.
- Eijkelboom, N.M., Swinkels, A.C.M., de Ruiter, J., Boom, R.M., Wilms, P.F.C., Schutyser, M.A.I., 2023b. High-resolution thermography and modelling allows for improved characterization of drying sessile single droplets. *J. Food Eng.* 341. <https://doi.org/10.1016/j.jfoodeng.2022.111340>.
- Finotello, G., De, S., Vrouwenvelder, J.C.R., Padding, J.T., Buist, K.A., Jongasma, A., Innings, F., Kuipers, J.A.M., 2018a. Experimental investigation of non-Newtonian droplet collisions: the role of extensional viscosity. *Exp. Fluid* 59 (7), 1–16. <https://doi.org/10.1007/S00348-018-2568-2/FIGURES/13>.
- Finotello, G., Kooiman, R.F., Padding, J.T., Buist, K.A., Jongasma, A., Innings, F., Kuipers, J.A.M., 2018b. The dynamics of milk droplet–droplet collisions. *Exp. Fluid* 59 (1), 17. <https://doi.org/10.1007/s00348-017-2471-2>.
- Fröhlich, J.A., Raiber, T.V., Hinrichs, J., Kohlus, R., 2021. Nozzle zone agglomeration in spray dryers: influence of total solid content on agglomerate properties. *Powder Technol.* 390, 292–302. <https://doi.org/10.1016/j.powtec.2021.05.094>.
- Fröhlich, J.A., Ruprecht, N.A., Kohlus, R., 2023. Nozzle zone agglomeration in spray dryers: determination of the agglomeration efficiency in the fines return by means of agglomerate properties and residence time distribution. *Dry. Technol.* <https://doi.org/10.1080/07373937.2023.2203224>.
- García Llamas, C., Swami, V.V., Timmermans, B.A.G., Buist, K.A., Kuipers, J.A.M., Baltussen, M.W., 2024. Numerical simulation of binary droplet collisions using a front tracking interface technique. *Chem. Eng. Sci.* 284, 119510. <https://doi.org/10.1016/j.ces.2023.119510>.
- Hunter, J.D., 2007. Matplotlib: a 2D graphics environment. *Comput. Sci. Eng.* 9 (3), 90–95. <https://doi.org/10.1109/MCSE.2007.55>.
- Hussain, F., Jaskulski, M., Piatkowski, M., Tsotsas, E., 2022. CFD simulation of agglomeration and coalescence in spray dryer. *Chem. Eng. Sci.* 247. <https://doi.org/10.1016/j.ces.2021.117064>.
- Kluyver, T., Ragan-Kelley, B., Pérez, F., Granger, B., Bussonnier, M., Frederic, J., Kelley, K., Hamrick, J., Grout, J., Corlay, S., Ivanov, P., Avila, D., Abdalla, S., Willing, C., 2016. Jupyter Notebooks—a publishing format for reproducible computational workflows. In: *Positioning and Power in Academic Publishing: Players, Agents and Agendas - Proceedings of the 20th International Conference on Electronic Publishing*. ELPUB, pp. 87–90. <https://doi.org/10.3233/978-1-61499-649-1-87>, 2016.
- Li, H., Kuschel, M., Sommerfeld, M., 2016. Experimental investigation and modeling of coalescence and agglomeration for spray drying of solutions. In: *Process-Spray: Functional Particles Produced in Spray Processes*. Springer International Publishing, pp. 205–233. https://doi.org/10.1007/978-3-319-32370-1_6.
- McKinney, W., 2010. Data structures for statistical computing in python. In: *Proceedings of the 9th Python in Science Conference*.
- Pawar, S.K., Henrikson, F., Finotello, G., Padding, J.T., Deen, N.G., Jongasma, A., Innings, F., Kuipers, J.A.M.H., 2016. An experimental study of droplet-particle collisions. In: *Powder Technology*, vol. 300. Elsevier B.V, pp. 157–163. <https://doi.org/10.1016/j.powtec.2016.06.005>.
- Perdana, J., Fox, M.B., Schutyser, M.A.I., Boom, R.M., 2013. Mimicking spray drying by drying of single droplets deposited on a flat surface. *Food Bioprocess Technol.* 6 (4), 964–977. <https://doi.org/10.1007/s11947-011-0767-4>.
- Qian, J., Law, C.K., 1997. Regimes of coalescence and separation in droplet collision. *J. Fluid Mech.* 331, 59–80. <https://doi.org/10.1017/S0022112096003722>.
- Räderer, M., Besson, A., Sommer, K., 2002. A thin film dryer approach for the determination of water diffusion coefficients in viscous products. *Chem. Eng. J.* 86. Seabold, S., Perktold, J., 2010. Statsmodels: econometric and statistical modeling with python. In: *Proceedings of the 9th Python in Science Conference*.
- Siemons, I., Politek, R.G.A., Boom, R.M., van der Sman, R.G.M., Schutyser, M.A.I., 2020. Dextrose equivalence of maltodextrins determines particle morphology development during single sessile droplet drying. *Food Res. Int.* 131. <https://doi.org/10.1016/j.foodres.2020.108988>.
- Siemons, I., Vesper, J., Boom, R.M., Schutyser, M.A.I., van der Sman, R.G.M., 2022. Rheological behaviour of concentrated maltodextrins describes skin formation and morphology development during droplet drying. *Food Hydrocolloids* 126, 107442. <https://doi.org/10.1016/j.foodhyd.2021.107442>.
- Terrazas-Velarde Korina, K., Peglow, M., Tsotsas, E., 2011. Kinetics of fluidized bed spray agglomeration for compact and porous particles. *Chem. Eng. Sci.* 66 (9), 1866–1878. <https://doi.org/10.1016/j.ces.2011.01.037>.
- van Boven, A.P., Calderon Novoa, S.M., Kohlus, R., Schutyser, M.A.I., 2023. Investigation on nozzle zone agglomeration during spray drying using response surface methodology. *Powder Technol.* 429, 118910. <https://doi.org/10.1016/j.powtec.2023.118910>.
- van Rossum, G., Drake, F.L., 1995. Python tutorial. Centrum Voor Wiskunde En Informatica Amsterdam 620.
- Virtanen, P., Gommers, R., Oliphant, T.E., Haberland, M., Reddy, T., Cournapeau, D., Burovski, E., Peterson, P., Weckesser, W., Bright, J., van der Walt, S.J., Brett, M., Wilson, J., Millman, K.J., Mayorov, N., Nelson, A.R.J., Jones, E., Kern, R., Larson, E., et al., 2020. SciPy 1.0: fundamental algorithms for scientific computing in Python. *Nat. Methods* 17 (3), 261–272. <https://doi.org/10.1038/s41592-019-0686-2>.
- Williams, A.M., Jones, J.R., Paterson, A.H.J., Pearce, D.L., 2009. Effect of fines on agglomeration in spray dryers: an experimental study. *Int. J. Food Eng.* 5 (2). <https://doi.org/10.2202/1556-3758.1635>.